Cross-caloric effect in multiferroic bismuth ferrite

Siyin Li,[1] Ningbo Fan,[1,*] L. Bellaiche,[2] and Bin Xu[1,†]

[1]*Jiangsu Key Laboratory of Frontier Material Physics and Devices, Institute of Theoretical and Applied Physics, School of Physical Science and Technology, Soochow University, Suzhou 215006, China*

[2]*Smart Ferroic Materials Center, Physics Department and Institute for Nanoscience and Engineering, University of Arkansas, Fayetteville, Arkansas 72701, USA*

(Received 24 December 2023; revised 13 May 2024; accepted 7 June 2024; published 21 June 2024)

Multiferroic materials consisting of multiple and mutually coupled order parameters including polarization can have an intriguing response to applied electric field, and give rise to the so-called cross-caloric effect, as the nondipolar degrees of freedom can contribute to the electrocaloric effect (ECE) via cross couplings to the electric dipoles. In this study, we use a first-principles-based effective Hamiltonian combined with Monte Carlo simulations to investigate such an effect systematically in the well-known room-temperature multiferroic system $BiFeO_3$ (BFO), in which there exists three coupled order parameters that can respond to electric field, i.e., polarization, octahedral tiltings, and antiferromagnetism. We adopt and compare three methods based on the cumulant formula, Maxwell relation, and a Landau model, respectively. The Landau approach allows the computation of decomposed contribution from each order parameter, and magnetism is found to contribute significantly to the ECE near the Néel temperature. The electrocaloric (EC) adiabatic temperature changes and the EC coefficients are computed with various field directions and magnitudes, with which sizable positive and negative ECE are found.

DOI: 10.1103/PhysRevB.109.214110

I. INTRODUCTION

Electrocaloric effect (ECE), with which a dielectric material can change its temperature via adiabatic application of an external electric field, is promising to be utilized in future solid-state refrigeration technologies, which can offer higher energy conversion efficiency and less environmental pollution compared with conventional vapor-compression refrigerators [1–6]. The ECE is usually achieved by the entropy variation of the electric dipoles under the influence of the field [6–10], while interestingly, recent studies demonstrated that multiferroic materials can allow an enhanced ECE thanks to the existence of multiple degrees of freedom (including polarization) and their mutual couplings, for instance, in $SrMnO_3$ and $BiCoO_3$ that are magnetoelectric systems [11,12] and $EuTiO_3$ thin films that is due to misfit strain and external mechanical stress [13]. In contrast to the multicaloric effect that requires applications of more than one types of driving field, the ECE in systems with multiple order parameters responding to the electric field can be called cross-caloric effect.

$BiFeO_3$ (BFO) is the most widely studied room-temperature multiferroic material. It crystallizes in a perovskite structure whose ground state is of the rhombohedral *R3c* symmetry with a large polarization along the [111] direction (approximately 90 $\mu C/cm^2$) and a Curie temperature of $T_C \approx 1100$ K. The *R3c* structure also possesses antiphase octahedral tilting ω_R in the same direction as polarization, i.e., $a^-a^-a^-$ in Glazer's notation. The magnetic ground state of bulk BFO is approximately G-type antiferromagnetic (G-AFM) with a Néel temperature T_N of about 640 K, but the magnetic moments form a spin cycloid along the $[1\bar{1}0]$ direction with a long period of about 62–64 nm [14–16]. However, the cycloidal state is destroyed and changes into G-AFM with weak ferromagnetization when BFO is subject to sufficiently large external electric field [17], magnetic field [18], strain [19], pressure [20], or chemical substitution [21].

The ECE of the multiferroic rare-earth-substituted BFO in the *R3c* phase was studied in Ref. [22], in which a small peak of the EC coefficient α (also called EC strength, which is the derivative of the temperature with respect to electric field at constant entropy) was found around the Néel temperature being originated from the coupling between polarization and magnetism. However, the ECE in pure BFO has not been thoroughly investigated, and the following questions remain unanswered: (i) The adiabatic temperature change upon application of an electric field has not been reported. (ii) Can the magnetism have a large contribution to the ECE? (iii) The major structural distortion of the *R3c* phase, i.e., the antiphase octahedral tiltings, was not considered in previous studies. (iv) Besides the [111] field, the ECE from [001], and $[\bar{1}\bar{1}\bar{1}]$ fields, which are common for thin films and polarization reversal, respectively, remains elusive. In particular, it was known that applying a field opposite to the polarization can give rise to a negative electrocaloric effect, which can be combined with normal positive ECE in electrocaloric devices to achieve improved thermal effect [23–25].

In this paper, we attempt to answer these questions using a first-principles-based effective Hamiltonian scheme, combined with Monte Carlo simulations. Approaches based on the cumulant method, Maxwell relation, and the Landau

*Contact author: nbfan2019@foxmail.com
†Contact author: binxu19@suda.edu.cn

phenomenological theory are considered. All methods yield consistent ECE results, whilst the Landau approach allows us to separate and identify the specific contributions of different order parameters in multiferroic systems to the ECE. Substantial EC temperature change is found for BFO, especially a very large contribution from the magnetic degree of freedom spotted near T_N. We quantify the contribution from the antiphase tiltings, and further explain the negative ECE and the positive EC coefficient from the $[\bar{1}\bar{1}\bar{1}]$ field.

The organization of this paper is as follows. Section II describes the employed computational methods. In Sec. III, we present the responses of the relevant order parameters to the applied electric field, the EC coefficients, and temperature change under various field and temperature conditions; analyze the contributions from the order parameters; and compare the results from different methods. Finally, the study is summarized in Sec. IV.

II. METHODS

A. Effective Hamiltonian

The simulations of $BiFeO_3$ are based on the effective Hamiltonian developed in Ref. [26], which successfully reproduces the ground-state properties of the *R3c* phase [27,28], the magnetoelectric coefficients, and the BFO domain patterns [29]. The total energy of BFO can be expressed as a sum of three parts:

$$E_{\mathrm{BFO}} = E^{\mathrm{FE}}(\{\boldsymbol{u}_i\},\{\eta_l\}) + E^{\mathrm{AFD}}(\{\boldsymbol{u}_i\},\{\eta_l\},\{\boldsymbol{\omega}_i\}) + E^{\mathrm{MAG}}(\{\boldsymbol{u}_i\},\{\eta_l\},\{\boldsymbol{\omega}_i\},\{\boldsymbol{m}_i\}), \quad (1)$$

where E^{FE} is the energy involving the local modes, elastic deformations, and their mutual couplings. E^{AFD} includes the energy contributions due to antiferrodistortive (AFD) motions and their interactions with local modes and strains, while E^{MAG} gathers the energies related to magnetic degrees of freedom and their couplings with other degrees of freedom.

This effective Hamiltonian contains four types of degrees of freedom: (i) the local modes $\{\boldsymbol{u}_i\}$ centered on the Bi ions, which are proportional to the local electric dipoles; (ii) the strain tensors $\{\eta_l\}$ including both the homogeneous and inhomogeneous strain [30,31]; (iii) the pseudovectors $\{\boldsymbol{\omega}_i\}$ that characterize the oxygen octahedral tiltings [32]; and (iv) the magnetic moment $\{\boldsymbol{m}_i\}$ of the Fe ions. More details about this method can be found in Ref. [33] and references therein.

The variations of the order parameters of $BiFeO_3$ at finite temperatures and under electric fields are simulated by Monte Carlo (MC) simulations based on this effective Hamiltonian, using a $12 \times 12 \times 12$ supercell (containing 8640 atoms). 20 000 MC sweeps are used for equilibration and another 20 000 sweeps are used to calculate the statistical averages. Under an applied electric field, an additional term $-\sum_i \boldsymbol{p}_i \cdot \boldsymbol{E}_i$ is incorporated, where the local electric dipoles $\boldsymbol{p}_i$ are computed from the local modes $\{\boldsymbol{u}_i\}$ and effective charges Z_i^*. Note that the theoretical critical field is typically much larger than that in the experiment as explained by Landauer's paradox [34]. Numerically, a factor of ~25 has been found in the *R3c* phase of BFO between our effective Hamiltonian predicted coercive field and experiment [35], but note that we do not perform rescaling in this study.

B. Method I: cumulant formula

We consider three approaches to calculate the field-induced adiabatic temperature change. In the first method, the EC coefficient can be computed directly based on MC simulations using the cumulant formula given in Ref. [22,36–38]:

$$\alpha_{\mathrm{cum}} = -Z^* a_{\mathrm{latt}} T \left\{ \frac{\langle |\boldsymbol{u}| E_{\mathrm{tot}} \rangle - \langle |\boldsymbol{u}| \rangle \langle E_{\mathrm{tot}} \rangle}{\langle E_{\mathrm{tot}}^2 \rangle - \langle E_{\mathrm{tot}} \rangle^2 + \frac{21(k_{\mathrm{B}}T)^2}{2N}} \right\}, \quad (2)$$

where Z^* is the Born effective charge associated with the local mode, a_{latt} represents the lattice constant of the five-atom pseudocubic perovskite cell, T is the simulation temperature, $|\boldsymbol{u}|$ is the supercell average of the magnitude of the local mode, E_{tot} is the total energy given by the effective Hamiltonian, k_{B} is the Boltzmann constant, N is the number of sites in the supercell, and $\langle\rangle$ denotes average over the MC sweeps at a given temperature.

With the EC coefficient obtained from the cumulant formula at various temperatures and electric fields, the EC temperature change can be computed with the following integral:

$$\Delta T = \int_{E_1}^{E_2} \alpha dE, \quad (3)$$

where E is electric field, and E_1, E_2 are the initial and final electric field, respectively.

C. Method II: Maxwell relation

The second method is often adopted in both experimental and theoretical studies, which is based on the Maxwell relation of thermodynamics $(\frac{\partial P}{\partial T})|_E = (\frac{\partial S}{\partial E})|_T$ that converts the isothermal entropy change to the change of the conjugate quantity of the electric field, i.e., the polarization [39]. With that, the EC adiabatic temperature change can be expressed as an integral of the pyroelectric coefficient:

$$\Delta T = -\int_{E_1}^{E_2} \frac{T}{C_E} \left(\frac{\partial P}{\partial T} \right) \Big|_E dE, \quad (4)$$

where E is electric field, E_1, E_2 are the initial and final electric field, respectively, T is temperature, P is the macroscopic polarization, and C_E is the specific heat under constant electric field. Note that C_E has field dependency (see Fig. 1), which can not be taken out of the integral in Eq. (4) [40]. The EC coefficient is in fact the integrand

$$\alpha_{\mathrm{Maxwell}} = -\frac{T}{C_E} \frac{\partial P}{\partial T} \Big|_E. \quad (5)$$

D. Method III: Landau model

The third method computes the entropy change directly from the Landau free energy. It does not involve the use of the Maxwell relation, and it has the advantage of allowing to quantify the separate ECE contribution from each order parameter. We consider the following Landau model [41,42]:

$$F = F_0 + \tfrac{1}{2}a_P(T)P^2 + \tfrac{1}{4}b_P P^4 - EP + \tfrac{1}{2}a_L(T)L^2 + \tfrac{1}{4}b_L L^4 + \tfrac{1}{2}a_{\omega_R}(T)\omega_R^2 + \tfrac{1}{4}b_{\omega_R}\omega_R^4 + c_1 P^2 L^2 + c_2 P^2 \omega_R^2 + c_3 L^2 \omega_R^2, \quad (6)$$

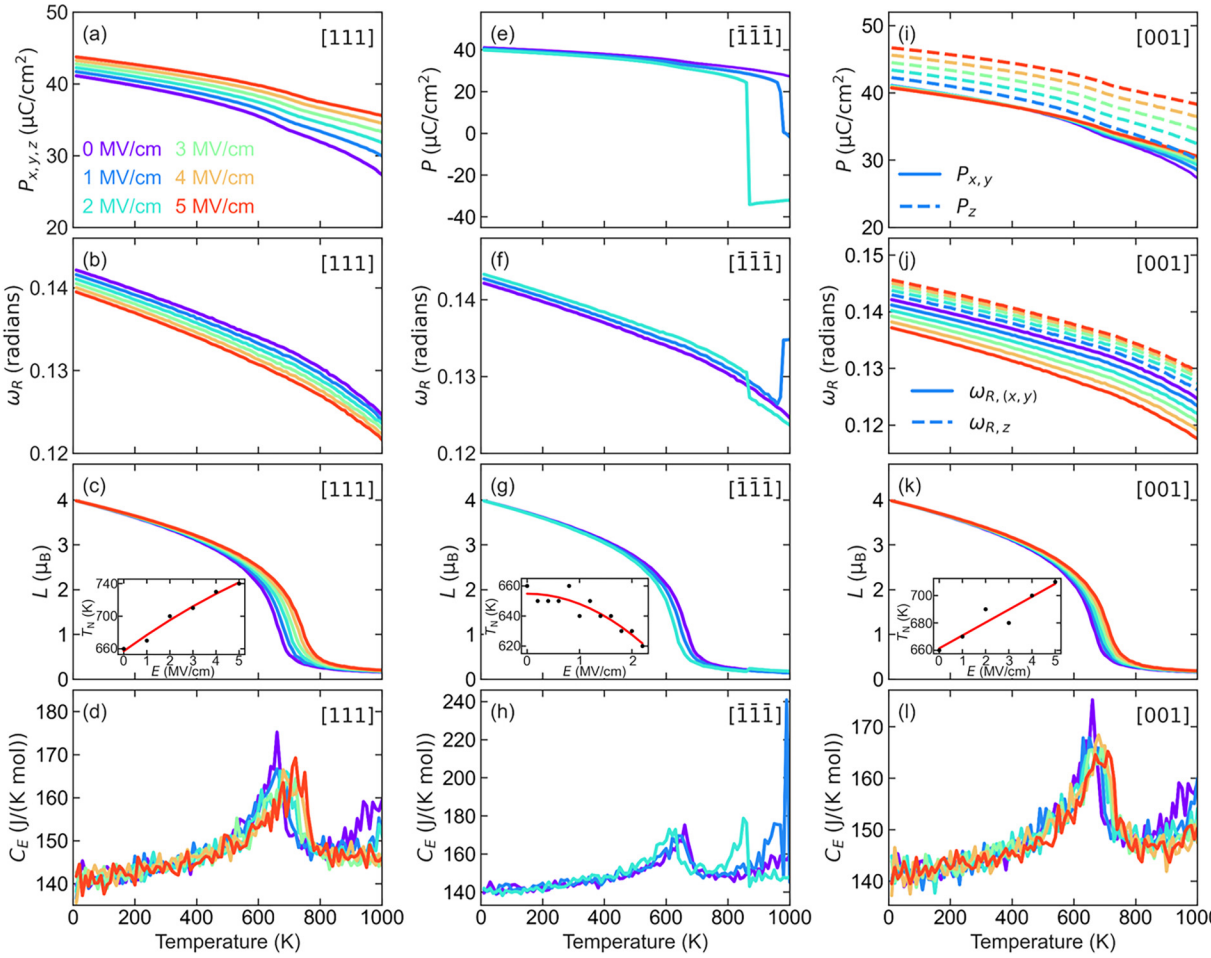

FIG. 1. Effect of E field on the order parameters and the specific heat as a function of temperature. (a)–(c) [111] field of 0–5 MV/cm. (e)–(g) [$\bar{1}\bar{1}\bar{1}$] field of 0–2 MV/cm. (i)–(k) [001] field of 0–5 MV/cm. The three relevant order parameters are polarization P, antiphase octahedral tilting ω_R, and antiferromagnetic moment L. Note that $P_x = P_y \neq P_z$ and $\omega_{R,x} = \omega_{R,y} \neq \omega_{R,z}$ for the [001] field. (d), (h), and (l) The response of system heat capacity to temperature under different electric field directions. The insets in (c), (f), and (i) shows the field dependence of T_N.

where F_0 is the constant part of the free energy, and three types of order parameters (ops) are considered, viz., the polarization P, antiphase octahedral tilting ω_R, and the magnitude of the G-AFM moment L. Note that only the magnitude of each op is used in the model, since the only temperature dependence is assumed to be in the quadratic coefficients, such that each op's components contribute equally, i.e., $\text{op}^2 = \text{op}_x^2 + \text{op}_y^2 + \text{op}_z^2$. The quadratic coefficient $a_{\text{op}} = A_{\text{op}}(T - T_0^{\text{op}})$ has explicit temperature dependence, and T_0^{op} is the transition temperature for the corresponding order parameter. The last three terms are the mutual biquadratic couplings between op pairs, allowing the response of octahedral tiltings and magnetism to the electric field. Recalling that $S = -\frac{\partial F}{\partial T}|_{E,\text{op}}$, the change of entropy associated with the application of an electric field can be expressed as

$$\begin{aligned}\Delta S = &-\tfrac{1}{2}A_P[P^2(T,E_2) - P^2(T,E_1)] \\ &-\tfrac{1}{2}A_L[L^2(T,E_2) - L^2(T,E_1)] \\ &-\tfrac{1}{2}A_{\omega_R}\left[{\omega_R}^2(T,E_2) - {\omega_R}^2(T,E_1)\right] \\ &= \Delta S_P + \Delta S_L + \Delta S_{\omega_R}, \end{aligned} \tag{7}$$

where E_1 and E_2 are the initial and final electric field, and the last line in Eq. (7) indicates that the total entropy change in BFO can be divided into individual contributions from P, L, and ω_R. The adiabatic EC temperature change can then be computed and divided into separate contributions as

$$\Delta T = -\frac{T}{C_E}\Delta S = \Delta T_P + \Delta T_L + \Delta T_{\omega_R}. \tag{8}$$

The EC coefficient can be further derived according to $\alpha = \Delta T/\Delta E$:

$$\begin{aligned}\alpha_{\text{LD}} = &\frac{TA_P}{2C_E\Delta E}[P^2(T,E_2) - P^2(T,E_1)] \\ &+ \frac{TA_L}{2C_E\Delta E}[L^2(T,E_2) - L^2(T,E_1)] \\ &+ \frac{TA_{\omega_R}}{2C_E\Delta E}\left[\omega_R^2(T,E_2) - \omega_R^2(T,E_1)\right] \\ &= \alpha_P + \alpha_L + \alpha_{\omega_R}\,. \end{aligned} \tag{9}$$

Here $E_1 = E - 1/2\Delta E$, $E_2 = E + 1/2\Delta E$, and ΔE is small as compared with E. The coefficients A_{op} can be

extracted by fitting $\alpha_{\rm cum}$ to $\alpha_{\rm LD}$ in Eq. (9), considering $A_{\rm op}$ as fitting parameters [38].

Note that the G-AFM state is considered in this study, while the cycloidal state is expected to have a similar ECE performance, because the quadratic coefficients are the same for the cycloidal and G-AFM states, and typically only these coefficients are temperature dependent. Moreover, the long period of the cycloid renders a local magnetic structure that is very close to G-AFM, and the most significant ECE contribution from the magnetic degrees of freedom is around the Néel temperature, around which the cycloid period further increases [43], thus the difference between the cycloid and the G-AFM state diminishes near the Néel temperature.

III. RESULTS

A. Responses of the order parameters to *E* field

Let us first check the effect of electric field on the three order parameters in Eq. (6) at various temperatures, as shown in Fig. 1. The temperature range is limited up to 1000 K, as we focus on the magnetoelectric effect on ECE in the *R3c* phase of BFO without structural phase transitions. Three field directions are considered, i.e., [111] being along the direction of the spontaneous polarization, $[\bar{1}\bar{1}\bar{1}]$ being opposite to the polarization direction, and [001] that is common for (001) film. The largest applied field of 5 MV/cm corresponds to 200 kV/cm considering the scale factor, when compared with experiments.

For [111] fields, the polarization increases under the field of the same direction, and the increment enlarges with temperature [Fig. 1(a)]. On the other hand, the antiphase tilting ω_R decreases slightly with the electric field. The opposite responses from P and ω_R are due to the competitive coupling between them [44]. The magnitude of the AFM vector L and the Néel temperature $T_{\rm N}$ increase under the influence of the field due to the collaborative coupling in the form of P^2L^2 [11], and the field dependence is close to being linear [inset of Fig. 1(c)].

If the field is applied along $[\bar{1}\bar{1}\bar{1}]$, i.e., opposite to the direction of the polarization, P decreases slightly before switching occurs [Fig. 1(e)]. The maximum field is limited not to go beyond 2 MV/cm, as ECE involving the switch process is not the focus of this study. The effect of the field on the antiphase tiltings is again opposite to that on the polarization, i.e., ω_R increases under the field [Fig. 1(f)]. Note that modulated nanotwin phase may occur for intermediate field [45], such as 1 MV/cm. On the other hand, L and $T_{\rm N}$ decrease when a $[\bar{1}\bar{1}\bar{1}]$ field is applied [Fig. 1(g)], as L^2 collaboratively couples to P^2.

Under a [001] field, the symmetry changes from rhombohedral *R3c* to monoclinic *Cc* such that the polarization is along a $[uuv]$ direction ($u < v$) and the antiphase tilting pseudovector is along $[u'u'v']$ ($u' < v'$). For polarization, the out-of-plane component P_z is significantly enhanced by the applied field, while the in-plane component P_x (or equivalently P_y) is much less sensitive except for high temperatures, i.e., above 600 K P_x (or P_y) slightly increases. The out-of-plane and in-plane components of ω_R show opposite changes under the [001] field: $\omega_{R,z}$ increases with the field whereas $\omega_{R,x}$ (or $\omega_{R,y}$) decreases. Since P increases, the field effect on L and $T_{\rm N}$ is similar as that for the [111] field, i.e., both of them increase.

The calculated specific heat C_E from MC simulations as a function of temperature at various fields are depicted in Figs. 1(d), 1(h), and 1(l). In general, C_E has relatively weak dependencies on temperature and electric field, except around the magnetic and structural phase transition points, where the specific heat peaks with an enhanced value. For conditions being away from the phase transitions, the computed values are close to that described by the Dulong-Petit law. These MC specific heat are used in the following calculations of the ECE temperature change, while it is worth noting that quantum effect is not considered here, hence the specific heat below room temperature is overestimated.

B. Contributions to the electrocaloric effect

To learn the behavior of the EC coefficient α under an applied field and to compare the three methods described in Sec. II, Fig. 2 depicts the calculated α as a function of temperature with an electric field of 2 MV/cm for three field directions. The three methods provide similar results for the general temperature dependence of α, while $\alpha_{\rm Maxwell}$ yields slightly larger numerical values than the other two approaches. The excellent agreement between $\alpha_{\rm cum}$ and $\alpha_{\rm LD}$ is expected since the parameters in the Landau model are obtained by fitting to $\alpha_{\rm cum}$. Nevertheless, all three methods indicate that, besides the overall increasing trend of α as a function of temperature, an obvious peak is observed around $T_{\rm N}$, which originates from the coupling between polarization and magnetism as was also found in Ref. [22] for Nd substituted BFO (BNFO), but it is worth noting that the peak in pure BFO [Fig. 2(a)] is more pronounced than that in BNFO. Furthermore, the "peak" behavior found in this work is different from the predicted anomaly at $T_{\rm N}$ in Ref. [46], which shows an abrupt increase of $|\Delta S|$. For $[\bar{1}\bar{1}\bar{1}]$ fields, we limit the maximum temperature to be 800 K, which is slightly below the temperature where polarization switching occurs but still above the Néel temperature. For the same applied field of 2 MV/cm, it is interesting to note that the $[\bar{1}\bar{1}\bar{1}]$ field yields the largest EC coefficient at $T_{\rm N}$ compared with the [111] and [001] fields, i.e., $\alpha_{\rm cum} = 4.99$ mK cm/kV at 630 K for the $[\bar{1}\bar{1}\bar{1}]$ field, $\alpha_{\rm cum} = 3.91$ mK cm/kV at 700 K for the [111] field, and $\alpha_{\rm cum} = 3.77$ mK cm/kV at 690 K for the [001] field. Also note that our test calculations indicate that adding small biaxial strain (e.g., -2% at which the G-AFM state is known to be the ground state) has only a small effect on the EC coefficient.

With the Landau approach, we are able to compute the decomposed contributions to α from order parameter P, L, and ω_R, which are also shown in Fig. 2 (dashed lines). One can see that α_P is the main contribution, which increases monotonically with temperature; on the other hand, α_L is only significant around $T_{\rm N}$ and diminishes very quickly with temperatures away from $T_{\rm N}$. It is remarkable to note that the magnitude of α_L at $T_{\rm N}$ reaches a comparable value compared with α_P (1.84 vs 2.19 mK cm/kV for the [111] field, 2.19 vs 3.82 mK cm/kV for the $[\bar{1}\bar{1}\bar{1}]$ field, and 2.13 vs 2.88 mK cm/kV for the [001] field), indicating a strong magnetoelectric effect around the magnetic transition point. The contribution of α_{ω_R} was not considered in Ref. [22].

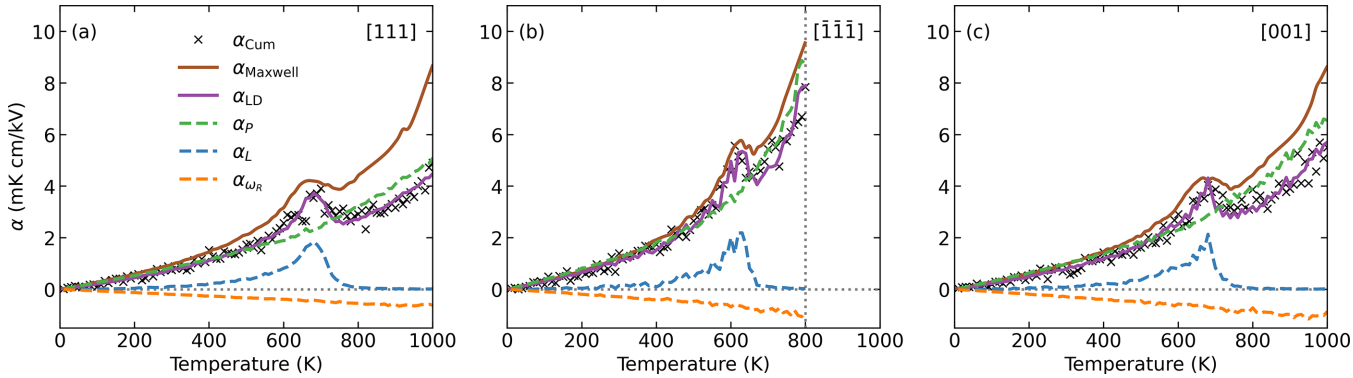

FIG. 2. Temperature dependence of the calculated α under various field directions with a field strength of 2 MV/cm for $BiFeO_3$. (a) [111]. (b) [$\bar{1}\bar{1}\bar{1}$]. (c) [001] electric field. The maximum temperature for the [$\bar{1}\bar{1}\bar{1}$] field is limited up to 800 K, since the ferroelectric to paraelectric transition or polarization switching occurs within the temperature range of 800–1000 K. α_{cum} (black crosses) is computed by the cumulant method, α_{LD} (violet solid lines) is computed by the Landau approach with decomposed contributions from α_P, α_L and α_{ω_R}. The brown solid lines represent α calculated using the Maxwell relation.

By including it explicitly we predict that it is negative and relatively small, with a nearly linear temperature dependence. The opposite sign of α_{ω_R} compared with α_P and α_L is due to its inverse response to the field (see Fig. 1). For the three field directions, one can notice that the contributions from L are similar, hence the larger α from the [$\bar{1}\bar{1}\bar{1}$] field than the other two field directions is mainly due to the contribution from polarization.

Assuming the initial field is zero and an electric field of 2 MV/cm is applied, Fig. 3 further illustrates the computed total adiabatic temperature change ΔT using three methods, i.e., cumulant method, Maxwell relation, and Landau model, and individual contributions from the latter approach are also shown. The overall results of ΔT of either the total temperature change or the decomposed contributions closely resemble those of α, since $\alpha = \delta T/\delta E$, but it is worth noting that ΔT is an integrated quantity from zero to E_{max} while α is evaluated at E_{max}. The peak value of ΔT around the Néel temperature is 8.33 K, −9.91 K, and 8.49 K for fields along [111], [$\bar{1}\bar{1}\bar{1}$], and [001], respectively, based on the Landau method. The largest ΔT comes from the [$\bar{1}\bar{1}\bar{1}$] field, which is primarily due to that fact that the Néel temperature is closer to the Curie temperature than the other two field directions.

The contribution of the magnetic subsystem, i.e., L, has a positive α_L or ΔT_L, indicating that it works collaboratively with the polarization, since these two order parameters couple via the $c_1 P^2 L^2$ term of Eq. (6) with a negative coefficient, and both become more ordered (increasing magnitudes) with the application of an electric field. The largest field effect on L is around the Néel temperature, giving rise to a peak ECE contribution from L.

The adiabatic temperature changes are positive for [111] and [001] fields, which correspond to the normal EC effect in ferroelectrics. However, ΔT is negative if the field is applied against the direction of the polarization (without switching the polarization), i.e., along [$\bar{1}\bar{1}\bar{1}$], and it has an inverse (or negative) EC effect [24,47]. Interestingly, the EC coefficient α is still positive [see Fig. 2(b)] for this field direction, since the positive field direction is chosen to be along the same direction as P (being consistent with the convention in P-E hysteresis loop), such that the change of field ΔE is negative. The differences in the magnitudes of ΔT calculated by

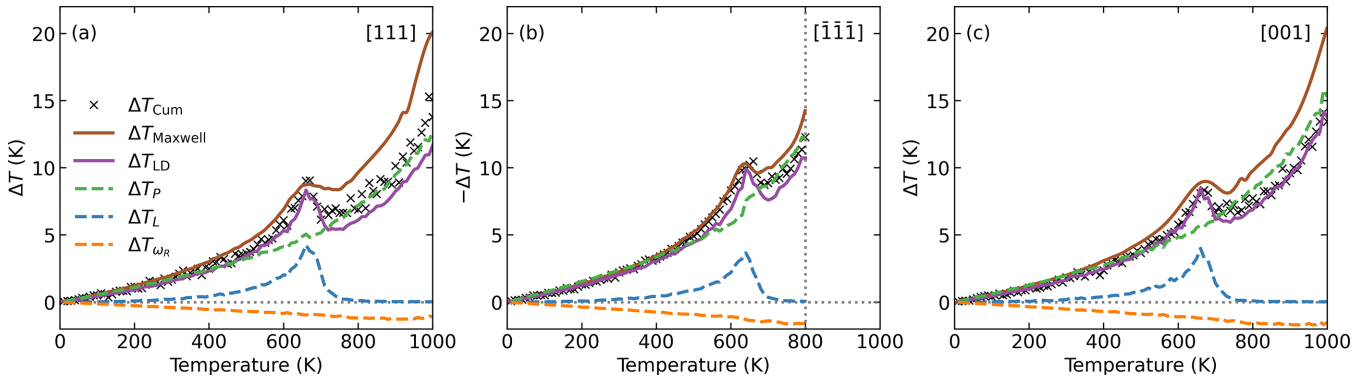

FIG. 3. The EC temperature change obtained using three methods under different electric field directions with a field strength of 2 MV/cm for $BiFeO_3$. (a) [111]. (b) [$\bar{1}\bar{1}\bar{1}$]. (c) [001] electric field. The change of temperature represented by the brown solid line is obtained using Maxwell relations Eq. (4). ΔT_{LD} (violet solid line), ΔT_P (green dashed line), ΔT_L (blue dashed line), and ΔT_{ω_R} (orange dashed line) are obtained by the Landau approach. ΔT_{cum} (black dotted line) is obtained by integrating α_{cum}.

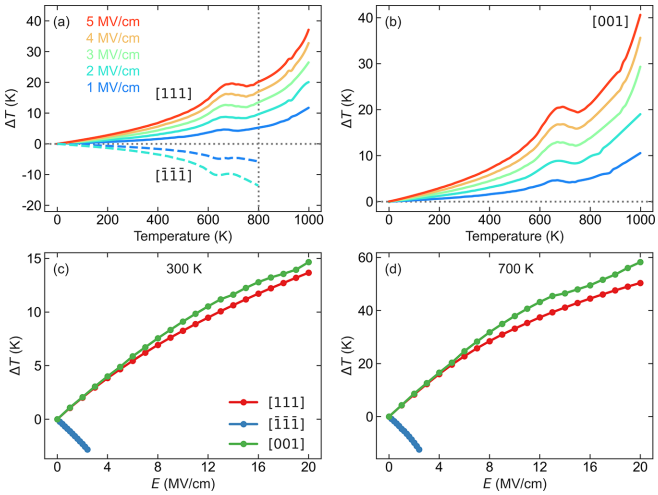

FIG. 4. Effect of the electric field strength on the EC temperature change in $BiFeO_3$. (a) Temperature dependence of the ΔT calculated by the Maxwell relation method with the [111] field (solid lines, 0–5 MV/cm) and [$\bar{1}\bar{1}\bar{1}$] (dashed lines, 0–2 MV/cm). (b) ibid for the [001] field (0–5 MV/cm). (c) and (d) Electric field dependence of EC temperature change at 300 K and 700 K, respectively.

different methods primarily stem from the discrepancies in the values of α obtained from Eq. (5) and Eq. (2), i.e., α_{Maxwell} is approximately 1.1–1.2 times that of α_{cum}.

C. ECE under various *E* fields

Magnitude of the applied electric field can strongly influence the EC temperature change. As shown in Fig. 4, ΔT as a function of temperature for various field strengths and three field directions are reported. Results obtained via the Maxwell relation method are presented, while we note that the values from the Landau approach are qualitatively similar. Overall, applying an electric field along the polarization direction (i.e., the [111] direction) results in a comparable ECE compared to that from the [001] field, whilst a field along the [$\bar{1}\bar{1}\bar{1}$] direction, i.e., against the polarization, yields a slightly more significant and negative thermal effect [Figs. 4(a) and 4(b)]. For instance, at 700 K and an applied electric field intensity of 2 MV/cm, the ΔT values for the [111], [001], and [$\bar{1}\bar{1}\bar{1}$] fields are 8.33 K, 8.66 K, and −9.86 K, respectively.

Furthermore, as the electric field magnitude increases, the ΔT is continuously enhanced with a sublinear relationship, in particular for large fields [see Figs. 4(c) and 4(d)]. At room temperature (300 K), the adiabatic temperature change can be as large as 13.67 K with a [111] field strength of 20 MV/cm (0.8 MV/cm after rescaling, see section A of the Methods), while at 700 K which is close to T_N the temperature change can reach 50.40 K with the same field strength. The sublinear behavior can be understood by the fact that T_C increases with increasing field, and concomitantly the pyroelectric coefficient $\frac{\partial P}{\partial T}$ decreases at the same temperature [see Figs. 1(a), (e), (i), and Eq. (4)]. For the [$\bar{1}\bar{1}\bar{1}$] field, note that we do not explore the case of a large field under which polarization switching occurs: In that case, the field direction is in the same direction as the polarization after switching and the electrocaloric effect is of the normal type (as in the [111] field case).

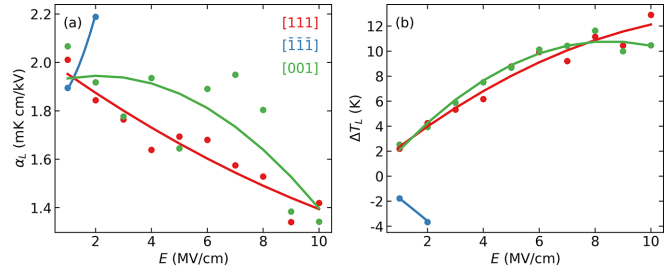

FIG. 5. The maximum magnetic contribution to ECE as a function of electric field. (a) α_L. (b) ΔT_L. Note that the maximum α_L occurs at T_N, while the maximum ΔT occurs at a slightly lower temperature. The solid lines are fitting curves of second-order polynomials.

It is of particular interest to understand how the contribution from magnetism varies with respect to the change of the field. Such contribution to the EC coefficient α_L and the EC temperature ΔT_L based on the Landau method are shown in Fig. 5. With increasing field, α_L of the [111] and [001] field decreases, while it increases for the [$\bar{1}\bar{1}\bar{1}$] field. Interestingly, opposite field dependencies are found for ΔT_L (similar to the total temperature change ΔT in Fig. 4), which is due to the fact that the adiabatic temperature is a cumulative quantity that can be related to α_L by $\Delta T = \int_0^{E_{\max}} \alpha dE$.

IV. SUMMARY

In summary, we have systematically studied the crossed caloric effect in multiferroic $BiFeO_3$ using three methods, viz., the cumulant method, Maxwell relation, and the Landau potential, based on Monte Carlo simulations, all with a first-principles-based effective Hamiltonian scheme. The various methods yield qualitatively consistent results, while the Landau approach allows quantification of the individual contribution to ECE from each order parameter. By considering two structural and one magnetic order parameters, i.e., polarization P, antiphase octahedral tilting ω_R, and antiferromagnetic moment L, we find that magnetism can have a significant contribution to ECE around the Néel temperature, causing a peak value of the overall ECE, while the effect from octahedral tiltings is relatively small. The ECE effect from three field directions and various magnitudes are also studied: Similar ECE are found for [111] and [001] fields, but for the [$\bar{1}\bar{1}\bar{1}$] field that is opposite to the polarization direction we show that it has a negative ECE and positive EC coefficient.

ACKNOWLEDGMENTS

This work is supported by the National Natural Science Foundation of China (Grant No. 12074277), Projects of International Cooperation and Exchanges NSFC (Grant No. 12311530693), Jiangsu Shuangchuang Project (JSSCTD202209), and the Priority Academic Program Development (PAPD) of Jiangsu Higher Education Institutions.

L.B. thanks the Office of Naval Research for support under Grant No. N00014-21-1-2086 and the Vannevar Bush Faculty Fellowship (VBFF) Grant No. N00014-20-1-2834 from the Department of Defense.

[1] T. Correlia and Q. Zhang, *Electrocaloric materials: new generation of coolers* (Springer, Berlin, 2014).

[2] G. G. Guzmán-Verri and P. B. Littlewood, Why is the electrocaloric effect so small in ferroelectrics? APL Mater. **4**, 064106 (2016).

[3] X. Moya, S. Kar-Narayan, and N. D. Mathur, Caloric materials near ferroic phase transitions, Nat. Mater. **13**, 439 (2014).

[4] J. Shi, D. Han, Z. Li, L. Yang, S.-G. Lu, Z. Zhong, J. Chen, Q. Zhang, and X. Qian, Electrocaloric cooling materials and devices for zero-global-warming-potential, high-efficiency refrigeration, Joule **3**, 1200 (2019).

[5] X. Moya and N. Mathur, Caloric materials for cooling and heating, Science **370**, 797 (2020).

[6] S. Fähler, U. K. Rößler, O. Kastner, J. Eckert, G. Eggeler, H. Emmerich, P. Entel, S. Müller, E. Quandt, and K. Albe, Caloric effects in ferroic materials: New concepts for cooling, Adv. Eng. Mater. **14**, 10 (2012).

[7] M. M. Vopson, The multicaloric effect in multiferroic materials, Solid State Commun. **152**, 2067 (2012).

[8] B. Neese, B. Chu, S.-G. Lu, Y. Wang, E. Furman, and Q. Zhang, Large electrocaloric effect in ferroelectric polymers near room temperature, Science **321**, 821 (2008).

[9] A. Mischenko, Q. Zhang, J. Scott, R. Whatmore, and N. Mathur, Giant electrocaloric effect in thin-film $PbZr_{0.95}Ti_{0.05}O_3$, Science **311**, 1270 (2006).

[10] X. Liu, Z. Wu, T. Guan, H. Jiang, P. Long, X. Li, C. Ji, S. Chen, Z. Sun, and J. Luo, Giant room temperature electrocaloric effect in a layered hybrid perovskite ferroelectric:$[(CH_3)_2CHCH_2NH_3]_2PbCl_4$, Nat. Commun. **12**, 5502 (2021).

[11] A. Edström and C. Ederer, Prediction of a giant magnetoelectric cross-Caloric effect around a tetracritical point in multiferroic $SrMnO_3$, Phys. Rev. Lett. **124**, 167201 (2020).

[12] C. Cazorla and J. Íñiguez, Giant direct and inverse electrocaloric effects in multiferroic thin films, Phys. Rev. B **98**, 174105 (2018).

[13] Y.-Q. Zhao and H.-X. Cao, Multicaloric effect in multiferroic $EuTiO_3$ thin films, J. Mater. Sci. **55**, 5705 (2020).

[14] I. Sosnowska, T. P. Neumaier, and E. Steichele, Spiral magnetic ordering in bismuth ferrite, J. Phys. C: Solid State Phys. **15**, 4835 (1982).

[15] G. Catalan and J. F. Scott, Physics and applications of bismuth ferrite, Adv. Mater. **21**, 2463 (2009).

[16] D. Lebeugle, D. Colson, A. Forget, M. Viret, A. Bataille, and A. Gukasov, Electric-field-induced spin flop in $BiFeO_3$ single crystals at room temperature, Phys. Rev. Lett. **100**, 227602 (2008).

[17] P. Rovillain, R. De Sousa, Y. Gallais, A. Sacuto, M. Méasson, D. Colson, A. Forget, M. Bibes, A. Barthélémy, and M. Cazayous, Electric-field control of spin waves at room temperature in multiferroic $BiFeO_3$, Nat. Mater. **9**, 975 (2010).

[18] M. Tokunaga, M. Azuma, and Y. Shimakawa, High-field study of strong magnetoelectric coupling in single-domain crystals of $BiFeO_3$, J. Phys. Soc. Jpn. **79**, 064713 (2010).

[19] D. Sando, A. Agbelele, D. Rahmedov, J. Liu, P. Rovillain, C. Toulouse, I. Infante, A. Pyatakov, S. Fusil, E. Jacquet *et al.*, Crafting the magnonic and spintronic response of $BiFeO_3$ films by epitaxial strain, Nat. Mater. **12**, 641 (2013).

[20] J. Buhot, C. Toulouse, Y. Gallais, A. Sacuto, R. De Sousa, D. Wang, L. Bellaiche, M. Bibes, A. Barthélémy, A. Forget *et al.*, Driving spin excitations by hydrostatic pressure in $BiFeO_3$, Phys. Rev. Lett. **115**, 267204 (2015).

[21] I. Sosnowska, W. Schäfer, W. Kockelmann, K. Andersen, and I. Troyanchuk, Crystal structure and spiral magnetic ordering of $BiFeO_3$ doped with manganese, Appl. Phys. A **74**, s1040 (2002).

[22] Z. Jiang, B. Xu, S. Prosandeev, Y. Nahas, S. Prokhorenko, J. Íñiguez, and L. Bellaiche, Electrocaloric effects in multiferroics, Phys. Rev. B **103**, L100102 (2021).

[23] M. Marathe, D. Renggli, M. Sanlialp, M. O. Karabasov, V. V. Shvartsman, D. C. Lupascu, A. Grünebohm, and C. Ederer, Electrocaloric effect in $BaTiO_3$ at all three ferroelectric transitions: Anisotropy and inverse caloric effects, Phys. Rev. B **96**, 014102 (2017).

[24] A. Grünebohm, Y.-B. Ma, M. Marathe, B.-X. Xu, K. Albe, C. Kalcher, K.-C. Meyer, V. V. Shvartsman, D. C. Lupascu, and C. Ederer, Origins of the inverse electrocaloric effect, Energy Technol. **6**, 1491 (2018).

[25] Y.-B. Ma, N. Novak, J. Koruza, T. Yang, K. Albe, and B.-X. Xu, Enhanced electrocaloric cooling in ferroelectric single crystals by electric field reversal, Phys. Rev. B **94**, 100104(R) (2016).

[26] D. Rahmedov, D. Wang, J. Íniguez, and L. Bellaiche, Magnetic cycloid of $BiFeO_3$ from atomistic simulations, Phys. Rev. Lett. **109**, 037207 (2012).

[27] D. Wang, J. Weerasinghe, and L. Bellaiche, Atomistic molecular dynamic simulations of multiferroics, Phys. Rev. Lett. **109**, 067203 (2012).

[28] B. Xu, B. Dupé, C. Xu, H. Xiang, and L. Bellaiche, Revisiting spin cycloids in multiferroic $BiFeO_3$, Phys. Rev. B **98**, 184420 (2018).

[29] Y. Nahas, S. Prokhorenko, J. Fischer, B. Xu, C. Carrétéro, S. Prosandeev, M. Bibes, S. Fusil, B. Dkhil, V. Garcia *et al.*, Inverse transition of labyrinthine domain patterns in ferroelectric thin films, Nature (London) **577**, 47 (2020).

[30] W. Zhong, D. Vanderbilt, and K. M. Rabe, Phase transitions in $BaTiO_3$ from first principles, Phys. Rev. Lett. **73**, 1861 (1994).

[31] W. Zhong and D. Vanderbilt, Competing structural instabilities in cubic perovskites, Phys. Rev. Lett. **74**, 2587 (1995).

[32] I. A. Kornev, L. Bellaiche, P.-E. Janolin, B. Dkhil, and E. Suard, Phase diagram of $Pb(Zr,Ti)O_3$ solid solutions from first principles, Phys. Rev. Lett. **97**, 157601 (2006).

[33] B. Xu, D. Wang, J. Íñiguez, and L. Bellaiche, Finite-temperature properties of rare-earth-substituted $BiFeO_3$ multiferroic solid solutions, Adv. Funct. Mater. **25**, 552 (2015).

[34] R. Landauer, Electrostatic considerations in $BaTiO_3$ domain formation during polarization reversal, J. Appl. Phys. **28**, 227 (1957).

[35] C. Daumont, W. Ren, I. Infante, S. Lisenkov, J. Allibe, C. Carrétéro, S. Fusil, E. Jacquet, T. Bouvet, F. Bouamrane *et al.*, Strain dependence of polarization and piezoelectric response in epitaxial $BiFeO_3$ thin films, J. Phys.: Condens. Matter **24**, 162202 (2012).

[36] Z. Jiang, S. Prokhorenko, S. Prosandeev, Y. Nahas, D. Wang, J. Íñiguez, E. Defay, and L. Bellaiche, Electrocaloric effects in the lead-free Ba(Zr, Ti)O_3 relaxor ferroelectric from atomistic simulations, Phys. Rev. B **96**, 014114 (2017).

[37] Z. Jiang, Y. Nahas, S. Prokhorenko, S. Prosandeev, D. Wang, J. Íñiguez, and L. Bellaiche, Giant electrocaloric response in the prototypical Pb(Mg, Nb)O_3 relaxor ferroelectric from atomistic simulations, Phys. Rev. B **97**, 104110 (2018).

[38] N. Fan, J. Iniguez, L. Bellaiche, and B. Xu, Origin of negative electrocaloric effect in Pnma-type antiferroelectric perovskites, Phys. Rev. B **106**, 224107 (2022).

[39] A. Planes, T. Castan, and A. Saxena, Thermodynamics of multicaloric effects in multiferroics, Philos. Mag. **94**, 1893 (2014).

[40] M. Marathe, A. Grünebohm, T. Nishimatsu, P. Entel, and C. Ederer, First-principles-based calculation of the electrocaloric effect in $BaTiO_3$: A comparison of direct and indirect methods, Phys. Rev. B **93**, 054110 (2016).

[41] Z. Kutnjak, B. Rožič, and R. Pirc, Electrocaloric effect: theory, measurements, and applications, *Wiley Encyclopedia of Electrical and Electronics Engineering*, edited by J. G. Webster (Wiley, 2015).

[42] D. V. Karpinsky, E. A. Eliseev, F. Xue, M. V. Silibin, A. Franz, M. D. Glinchuk, I. O. Troyanchuk, S. A. Gavrilov, V. Gopalan, L.-Q. Chen *et al.*, Thermodynamic potential and phase diagram for multiferroic bismuth ferrite ($BiFeO_3$), npj Comput. Mater. **3**, 20 (2017).

[43] M. Ramazanoglu, W. Ratcliff, II, Y. J. Choi, S. Lee, S.-W. Cheong, and V. Kiryukhin, Temperature-dependent properties of the magnetic order in single-crystal $BiFeO_3$, Phys. Rev. B **83**, 174434 (2011).

[44] P. Marton, A. Klíč, M. Paściak, and J. Hlinka, First-principles-based Landau-Devonshire potential for $BiFeO_3$, Phys. Rev. B **96**, 174110 (2017).

[45] S. Prosandeev, D. Wang, W. Ren, J. Íñiguez, and L. Bellaiche, Novel nanoscale twinned phases in perovskite oxides, Adv. Funct. Mater. **23**, 234 (2013).

[46] X.-S. Cao, Electrocaloric effect anomaly in multiferroic $BiFeO_3$, Mater. Res. Express **6**, 076112 (2019).

[47] M. Graf and J. Íñiguez, A unified perturbative approach to electrocaloric effects, Commun. Mater. **2**, 60 (2021).